URURSI AP-RASC, Sydney, Australia, 17 – 22 August 2025

A Backed-Cavity Silver Screen-Printed Spiral Antenna with Integrated Solar Cells for Autonomous IoT Nodes

Leonardo Pierantozzi[#], Giacomo Schiavolini[#], Valentina Palazzi[#], Roberto Vincenti Gatti[#], Marco Galiazzo*, Davide Colla*, and Paolo Mezzanotte [#]
Applied Materials (AMAT)*
University of Perugia[#]

Abstract

In this article a wide band antenna with solar cells-based energy harvesting capabilities for Internet-of-Things systems is presented. The antenna is realized by exploiting an Archimedean coil made through silver screen printing technology on a polycarbonate substrate. Thanks to this fabrication method, the operating bandwidth extends from 0.7 GHz to 2.5 GHz. The solar cells are positioned at the base of the metal cavity. The antenna characterization shows a maximum gain of 10 dBi, with 450 mW of generated DC-power. An IoT node composed of the spiral antenna is illustrated, comprehensive of a DC-DC converter, a control circuit and a transceiver able to connect to the LTE-M network.

1. Introduction

Nowadays, the Internet of Things (IoT) scenario depicts novel engineering challenges for the architecture realization. Among several key aspects for these devices, the high connectivity is becoming a non-negligible factor for the antenna design [1,2]. These antennas must be capable of supporting different communication standards, such as 5G, Wi-Fi, and Bluetooth, to accommodate a wide range of IoT applications, which imply a wide-band operation. Alongside connectivity, energy harvesting has emerged as a key technology. Many IoT applications, especially those in remote or hard-to-reach locations, require power sources that are both efficient and sustainable. There are multiple types of energy sources that can be leveraged for powering IoT systems, such as solar radiation, wind, mechanical vibrations, temperature gradients, and ambient radio-frequency signals. For example, in [3], a multiband ambient RF energy harvesting circuit has been demonstrated, capable of powering battery less sensors and IoT devices in the 700–900 MHz range, illustrating the feasibility of maintenance-free operation. Another relevant approach is described in [4], which presents a gravitational electromagnetic energy harvester designed to power an IoT node on freight train wagons.
Energy harvesting, which captures and stores energy from environmental sources such as light, offers another promising alternative, enabling devices to run autonomously for extended periods without the need for frequent battery replacements. In this context, the integration of wide-band antenna technologies and energy harvesting solutions is essential to support the growing demand for IoT devices that are both high-performing and energy-efficient.
In this paper, a wide band backed cavity silver screen printed spiral antenna is presented, which covers multiple frequency standards. The operational bandwidth spans from 0.7 GHz to 2.5 GHz, while circular polarization is used to avoid polarization mismatches. The metallic cavity is employed to realize a monodirectional radiation pattern, but it helps to minimize the antenna performance degradation due to the metallic environment. In fact, the cavity is carefully shaped to be collocated into a metallic container corrugation, typically used for intermodal transportation. To integrate solar cells on the inner side of cavity, the Archimedean spiral is printed on a polycarbonate substrate, which allows sunlight to reach the solar cells. The realization of spiral trace on this substrate, an innovative silver screen printing technique is adopted. In section 2 is discussed the antenna design and characterization, while in section 3 the solar cells' integrations and characterization is presented. Finally, in section 4 the results achieved are shown, along with the state-of-the-art (SoA) comparison.

2. Antenna Design

To make the antenna cover the required ultra-wideband, we developed a backed cavity spiral antenna with an absorbing material [5,6]. By employing this solution, it is possible to satisfy all the design specifications, such as immunity from metallic environment on the bottom side and good directivity. The spiral design is based on theory explained [6], while the aluminum cavity dimensions are shaped accordingly to [5] and to the container corrugation size. All the design parameters have been optimized to find a compromise between performance and dimensions constraints. The main cavity dimensions are depicted in Figure 1, while the spiral parameters, printed with silver screen printing technique, can be summarized as follows. The inner radius is equal to 3 mm, line width is fixed to 8 mm, spiral progress is 20 with 3 coil turns. In this realization, the antenna spiral has been screen-printed on the internal side of polycarbonate substrate to ensure protection from the external environment conditions. The connection between the spiral and the coaxial cable has been formed by a deposition of an electrically conductive adhesive. Finally, the absorbing material creates an inner ring with 19 mm of thickness inside the cavity.

The antenna has been characterized in anechoic chamber to compare the measurements results along with the simulation, the main results are shown in Figure 2.

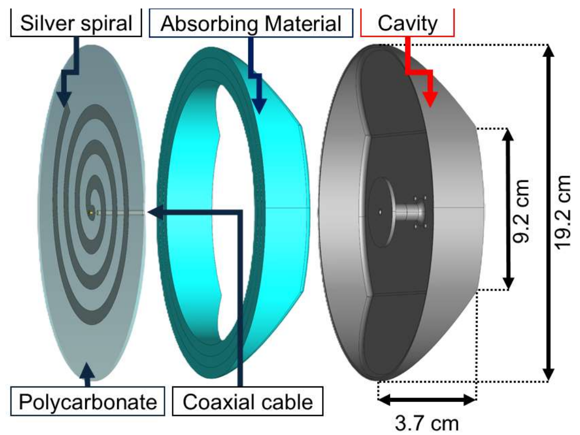

Figure 1. Exploded view of the proposed wideband antenna with integrated solar cells.

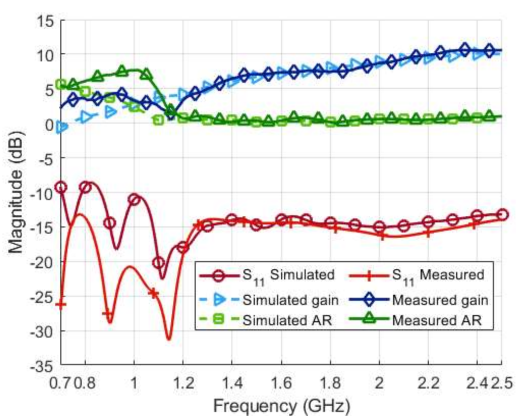

Figure 2. Simulations and measurements results comparisons respect to the antenna reflection coefficients, realized gain and axial ratio (AR).

The overall performances at high frequencies are in a good agreement with the simulation results. Some discrepancies can be found for frequencies below 1.1 GHz, where the reflection coefficient and the axial ratio are worse compared to the full-wave results. Moreover, at 1.1 GHz, for an unwanted main lobe, the antenna gain decreases on the boresight direction (see Figure 2). These performance degradations are caused by the backed cavity shaping, performed to meet the space requirements for the design. The performance compromise on gain and axial ratio degradation has been made to match the dimensional constraints for the antenna.

3. Solar Cell Integration

To achieve harvesting capabilities, the space inside the antenna has been exploited to place the six solar panels connected in parallel. The realized antenna is depicted in Figure 3, in which is employed embedded Component Off the Shelf (COTS) solar cells.

To evaluate the available output power of the six cells, it is crucial to perform an empirical characterization. The adopted setup to carry out these measurements is depicted in Figure 4. The setup is composed of the proposed antenna with integrated solar panels, a light meter, a set of variable loads, and a voltmeter. For each level of illuminance (lx), that is the total luminous flux incident on a surface per unit area, the voltmeter measured the panel's voltage across each load. The goal is to find the maximum power point (MPP). In Figure 5 the P-V curves are illustrated depending on different illuminance values. At the highest illuminance, the maximum power point is approximately 450 mW at a voltage of 1.7 V.

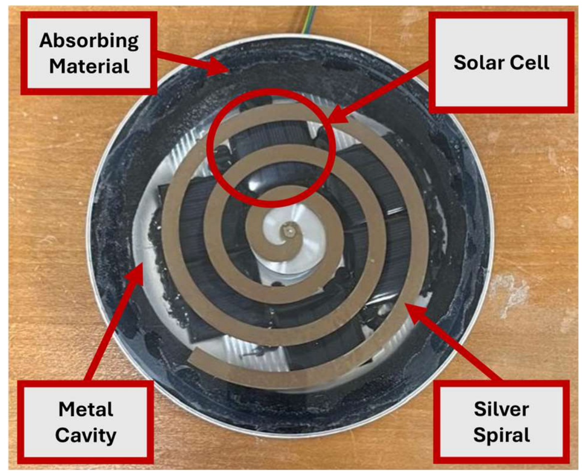

Figure 3. Antenna prototype with integrated solar cells.

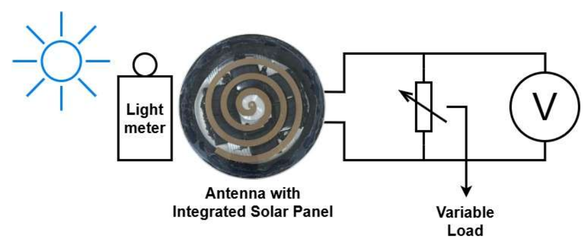

Figure 4. Schematic of the solar cells' characterization setup.

To evaluate the available output power of the six cells, it is crucial to perform an empirical characterization. The adopted setup to carry out these measurements is depicted in Figure 4. The setup is composed of the proposed antenna with integrated solar panels, a light meter, a set of variable loads, and a voltmeter. For each level of illuminance (lx), that is the total luminous flux incident on a surface per unit area, the voltmeter measured the panel's voltage across each load. The goal is to find the maximum power point (MPP). In Figure 5 the P-V curves are illustrated depending on different illuminance values. At the highest illuminance, the maximum power point is approximately 450 mW at a voltage of 1.7 V.

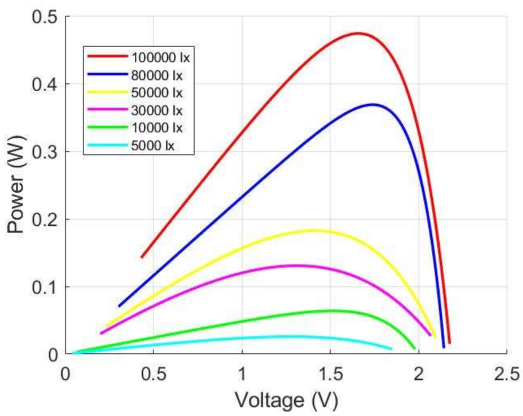

Figure 5. Power vs Voltage depending on different illuminance values

4. IoT Harvester and Transceiver

The complete IoT node is depicted in Figure 6, in which the schematic of the full system composed by the harvester and the transceiver is presented. Starting from the harvester, the solar panels are connected to a DC-DC boost converter (STEVAL-ISV006V2) which converts the panels output voltage into 4 V, that is the voltage required to activate the transceiver. At the converter output a 4 F capacitor is placed for storing the collected energy. By means of a command signal from the converter, the circuit located downstream of the capacitor can be controlled. Thus, the transceiver is powered only if the capacitor is charged. The transceiver is composed of an IoT module (HL7812) placed in a development board. It is connected to the antenna, and it is fed by the harvester. The IoT module can connect to the LTE-M (or LTE Cat-M1) network that is a technology standard for machine-to-machine and IoT applications. Using AT commands, it is possible to communicate with the module through a serial interface. By means of a Python script, the module sends a message to the user's phone, containing the RSSI (Receiver Signal Strength Indicator), the received power in dBm (calculated from RSSI), the active bands, the LAC (Location Area Code) and the Cell ID.

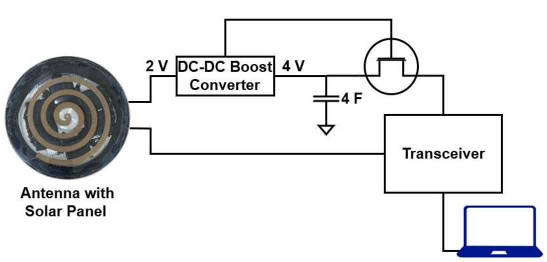

Figure 6. Schematic of the entire system

In Figures 7 and 8 the power consumption in two crucial scenarios are presented. The graphs are made by measuring a shunt resistor placed at the output of the DC-DC converter, by employing the Picoscope 2206B. Figure 7 illustrates the power consumption of the transceiver startup, which is divided into three parts. During the startup phase, the control circuit is activated, powering the transceiver. In the second phase the transceiver connects to the LTE-M network. Power consumption reaches peaks of approximately 130 mW, due to communication with the radio base station required to establish the connection. In the third period, the transceiver undergoes stabilization, during which several power consumption peaks occur before the device transitions to an idle phase. Figure 8 displays power consumption due to sending an SMS. The transceiver is connected and stable, hence it is in the idle phase, launching a python script the transceiver sends an SMS to the user's phone. In this stage, power consumption ranges from 40 mW to 130 mW and lasts approximately 5 seconds. Afterwards, a stabilization phase follows, as previously described.

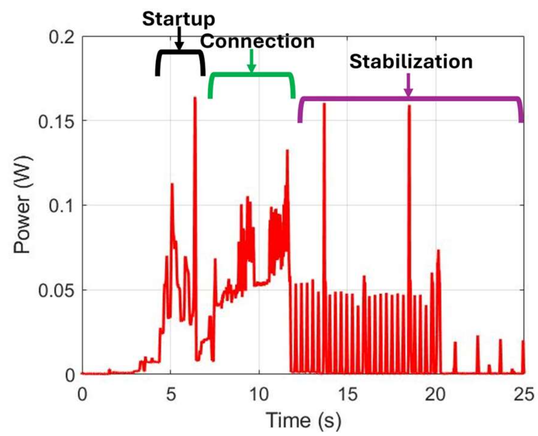

Figure 7. Transceiver startup power consumption

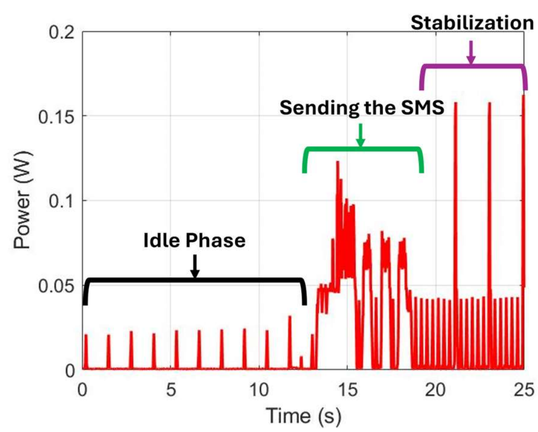

Figure 8. SMS sending transceiver power consumption

5.2 Conclusions

In this paper a wide band antenna based on backed cavity Archimedean silver screen printed spiral topology is presented. To achieve energy harvesting capabilities, six solar cells have been integrated at the bottom side of the metallic cavity. Even though the antenna results to be centered between 1.1-2.5 GHz, operational demonstrations have been performed down to 700 MHz. The antenna characterization in an anechoic chamber shows a gain that ranges from 2 to 10 dBi, depending on the operational frequency. The maximal axial ratio degradation is 5 dB and gain inflections are caused by the antenna size reduction due to dimensional constraints. The harvesting capabilities have been characterized, the peak DC-power provided by the antenna is equal to 450 mW at an illuminance of 100000 lx. To validate the entire IoT node, the antenna is connected to a radio for communicating through LTE-M protocol, while the solar cells are attached to a DC-DC converter and a capacitor to supply the radio electronics. In this way, the complete validation of autonomous IoT node with high connectivity communication system is provided. The performance from a power consumption point of view has been displayed, analyzing the transceiver startup and the operation of sending an SMS. Table 1 compares the proposed antenna with current state-of-the-art designs, showing that it achieves a wider bandwidth while maintaining a harvesting capability comparable to other reported solutions. Furthermore, this work presents a complete IoT node capable of operating autonomously from a power perspective.

Table 1 SoA Comparison

Ref.	BW [GHz]	Gain [dB]	P_{DC} [mW]	Area [cm^2]
[7]	2.08-4.1	1-4	438	155
[8]*	2.5-5	14-18	225	247
[9]*	1.26-3.2	14-18	9000#	1600
[This work]	0.7-2.5	0-10	450	290

* Array

$P_{DC} = V_{Open\_Circuit} \times I_{Short\_Circuit}$

6. Acknowledgements

This project has received funding from the ECSEL Joint Undertaking (JU) under grant agreement No 101007247. The JU receives support from the European Union's Horizon 2020 research and innovation programme and Finland, Germany, Ireland, Sweden, Italy, Austria, Iceland, Switzerland.

References

[1] S. Chen, H. Xu, D. Liu, B. Hu and H. Wang, "A Vision of IoT: Applications, Challenges, and Opportunities with China Perspective," in IEEE Internet of Things Journal, vol. 1, no. 4, pp. 349-359, Aug. 2014, doi: 10.1109/JIOT.2014.2337336.

[2] K. Shafique, B. A. Khawaja, F. Sabir, S. Qazi and M. Mustaqim, "Internet of Things (IoT) for Next-Generation Smart Systems: A Review of Current Challenges, Future Trends and Prospects for Emerging 5G-IoT Scenarios," in IEEE Access, vol. 8, pp. 23022-23040, 2020, doi: 10.1109/ACCESS.2020.2970118.

[3] U. Muncuk, K. Alemdar, J. D. Sarode and K. R. Chowdhury, "Multiband Ambient RF Energy Harvesting Circuit Design for Enabling Batteryless Sensors and IoT," in IEEE Internet of Things Journal, vol. 5, no. 4, pp. 2700-2714, Aug. 2018, doi: 10.1109/JIOT.2018.2813162.

[4] M. L. Monaco, C. Russo and A. Somà, "Investigation of Gravitational Energy Harvesters for IoT Power Supply in Freight Train Monitoring," 2023 25th European Conference on Power Electronics and Applications (EPE'23 ECCE Europe), Aalborg, Denmark, 2023, pp. P.1-P.8, doi: 10.23919/EPE23ECCEEurope58414.2023.10264497.

[5] H. Nakano, R. Satake and J. Yamauchi, "Extremely Low-Profile, Single-Arm, Wideband Spiral Antenna Radiating a Circularly Polarized Wave," in IEEE Transactions on Antennas and Propagation, vol. 58, no. 5, pp. 1511-1520, May 2010, doi: 10.1109/TAP.2010.2044345

[6] C. A. Balanis, Antenna Theory: Analysis and Design, New York: Wiley, pp. 611-619, 1982.

[7] Q. Chen et al., "A Broadband Active Solar Cell Meta-Surface Antenna," in IEEE Antennas and Wireless Propagation Letters, vol. 22, no. 9, pp. 2320-2324, Sept. 2023, doi: 10.1109/LAWP.2023.3287649.

[8] Q. Chen, Z. Li, W. Wang, Z. Huang, X. Liang and X. Wu, "A Broadband Dual-Polarized Solar Cell Phased Array Antenna," in IEEE Transactions on Antennas and Propagation, vol. 70, no. 1, pp. 353-364, Jan. 2022, doi: 10.1109/TAP.2021.3098520.

[9] X. -T. Sun, Q. Zhao, W. -Z. Lu and X. -C. Wang, "Optical Transparent Broadband Antenna Array Integrated With Polycrystalline Silicon Solar Cells," in IEEE Antennas and Wireless Propagation Letters, vol. 22, no. 2, pp. 248-252, Feb. 2023, doi: 10.1109/LAWP.2022.3208033.